

# Experimental and Analytical Investigation of a Modified Ring Cusp NSTAR Engine

IEPC-2005-160

Presented at the 29<sup>th</sup> International Electric Propulsion Conference, Princeton University,  
October 31 – November 4, 2005

Anita Sengupta\*  
Jet Propulsion Laboratory, Pasadena, CA, 91109, US

**Abstract:** A series of experimental measurements on a modified laboratory NSTAR engine were used to validate a zero dimensional analytical discharge performance model of a ring cusp ion thruster. The model predicts the discharge performance of a ring cusp NSTAR thruster as a function the magnetic field configuration, thruster geometry, and throttle level. Analytical formalisms for electron and ion confinement are used to predict the ionization efficiency for a given thruster design. Explicit determination of discharge loss and volume averaged plasma parameters are also obtained. The model was used to predict the performance of the nominal and modified three and four ring cusp 30-cm ion thruster configurations operating at the full power (2.3 kW) NSTAR throttle level. Experimental measurements of the modified engine configuration discharge loss compare well with the predicted value for propellant utilizations from 80 to 95%. The theory, as validated by experiment, indicates that increasing the magnetic strength of the first closed magnetic contour line reduces maxwellian electron diffusion and electrostatically confines the ion population and subsequent loss to the anode wall. The theory also indicates that increasing the cusp strength and minimizing the cusp area improves primary electron confinement increasing the probability of an ionization collision prior to loss at the cusp.

## Nomenclature

$n_{o,p,i,tot}$	= neutral, primary, maxwellian, ion, total electron number density
$R_L$	= Larmor radius
$\varepsilon_p, U_b, U_j$	= primary electron, ionization, excitation energy
$V_D, V_C$	= discharge voltage, cathode voltage
$A_{p,e}$	= primary, maxwellian magnetic cusp loss area
$L_{cusp}$	= magnetic cusp length
$t_p$	= primary electron confinement time
$V$	= discharge chamber volume
$v_{p,m,i}$	= primary electron, Maxwellian, ion velocity
$J_{P,M,ion,D,B,s,A}$	= primary electron, maxwellian electron, ion, discharge, beam, screen, anode current
$m_{e,Xe}$	= electron mass, xenon atomic mass
$B$	= magnetic field strength
$\nu, \tau$	= collision frequency and time
$\sigma_{o,i,excite}$	= total, ionization, excitation atomic cross section
$\lambda_m$	= mean free path
$d_{anode}$	= distance to anode
$D, \mu$	= diffusion and mobility coefficients
$P$	= power

---

\* Senior Engineer, Advanced Propulsion Technology, Anita.Sengupta@jpl.nasa.gov

$J_j$	=	total excited neutral production
$T_{e,o,i}$	=	electron, ion, neutral temperature
$\phi_i$	=	screen grid transparency to ions
$\phi_g$	=	screen grid open area fraction
$A_g$	=	grid area
$\eta_u$	=	propellant utilization
$k$	=	Boltzmann constant

## I. Introduction

Ion engines offer the potential for orders of magnitude performance improvement over traditional chemical propulsion systems, resulting in shorter trip times, reduced launch vehicle costs, and with the push for high power electric propulsion mission architectures, far more ambitious science return than ever before. In spite of the tremendous advantages the technology offers, actual use of the state-of-the-art ion thruster technology on NASA science missions has been limited, due to its insufficient electrical efficiency, high fabrication and test costs, and reliability/lifetime issues. The current inefficiencies of the state-of-the-art ion engine are directly related to the production and confinement of the discharge plasma in the engine's discharge (ionization) chamber. Poor plasma confinement is directly related to thruster lifetime, as non-uniform plasma production increases wear of the ion engines electrodes and electron source. Therefore an understanding of plasma production and confinement is critical to increasing efficiency, life, and reliability, of the ion thruster.

The state-of-the-art ion thruster, used on both the DS1 Mission and to be used on the Dawn mission, is the 30-cm-diameter NASA NSTAR thruster<sup>1,2</sup>. The NSTAR thruster is characterized by a ~60% total efficiency, 3000s Isp, and a lifetime of 235 kg of Xenon propellant throughput or 30,000 hours of operation<sup>3</sup>. The current and past research on the NSTAR ion thruster has predominantly focused on improving lifetime by understanding the wear mechanisms that lead to thruster failure for the nominal NSTAR thruster configuration. The life of the NSTAR thruster is primarily limited by erosion of the accelerator grid electrode<sup>4</sup>, erosion of the discharge cathode keeper, and depletion of the electron emitter source material<sup>3</sup>. Research focused on understanding the physical processes and/or plasma physics inside the thruster to improve overall performance and life, has however, been less emphasized. In many ways, these two research areas are intrinsically linked, in that design changes to improve thruster performance may impact thruster life, and vice versa. Improving the ionization efficiency of the thruster can reduce the discharge power requirements to run the hollow cathode, which in turn reduces the temperature at which it operates, increasing life of the emitter, and thereby increasing life of the thruster. Similarly, removing the non-uniformity of the plasma produced in the discharge chamber offers the potential to increase grid life by a factor of 2, which would increase the overall lifetime of the thruster and the total impulse that could be acquired per unit engine, requiring fewer engines to do the same mission. It is therefore a challenge with the potential for great rewards to the EP engineering community to improve the performance of the SOA NSTAR thruster.

The research activity described in this paper uses a combined approach of analytical model development of the bulk discharge plasma in conjunction with experimental measurements inside of an operating ion thruster, to quantitatively understand and improve upon the confinement and production of the discharge plasma. The spatially resolved Langmuir probe measurements are discussed in greater detail in Ref. 5. Results will be presented detailing the experimentally validated enhanced NSTAR thruster magnetic field configurations that improve ionization efficiency by up to 20% and plasma uniformity by up to 50%, significantly increasing the efficiency and lifetime of the NSTAR thruster. The model development in conjunction with experimental measurements, details the physics of magnetic electron and ion confinement, in a ring cusp geometry. The analytical model may also be used as a design tool for larger thrusters at different operating conditions, as it has no empirical based formulations, and only depends on a given thrusters geometry, magnetic circuit design, and throttle point.

## II. Discharge Plasma Confinement Theory

A zero dimensional analytical discharge performance model was developed to predict the thruster performance as a function of geometry, magnetic field, and operating conditions, without the need for empirical data or prior thruster testing. The model also details the physics of magnetic confinement of ions and electrons. The model explicitly defines plasma properties by their functional dependence on the throttle conditions, geometry, and

magnetic field. The goal was to create a model that is by definition scalable to larger thrusters, therefore serving as a predictive design tool to determine and optimize thruster performance.

### A. Plasma Production

There are several assumptions in the model to simplify the analytical formulations for a zero dimensional approach. It is assumed that there are two populations of electrons in the discharge chamber, a primary electron population emitted from the discharge cathode, and a Maxwellian population comprised of primaries that have undergone an inelastic collision and secondary electrons released in the ionization process. The primary electron current can be represented analytically by a monoenergetic electron distribution at the primary electron energy,  $\epsilon_p$ <sup>6</sup>. The primary electron energy is the difference between the discharge voltage and the cathode region plasma potential,  $V_c$ .

$$\epsilon_p = V_D - V_C \quad (1)$$

Primary electrons can lose their energy by collisional excitation, ionization, or recombination. Primary electron collisions with other electrons are assumed to be negligible, as the ion engine discharge is only partially ionized. Similarly, energy loss due to inelastic primary collisions with ions, are also assumed to be negligible. Energy loss from elastic primary electron collisions with neutrals and ions are also ignored, as such energy transfer is proportional to the ratio of the colliding particle masses. For Xenon this ratio is  $\sim 10^{-6}$ . In low pressure, partially ionized plasmas, ion-electron recombination occurs at the walls, and recombination in bulk plasma can be ignored. This is justified as the ion-electron collision frequency is an order of magnitude lower than the neutral-electron collision frequency, as the plasma is only 10% ionized. Consequently, both electrons and ions are assumed to be lost to thruster surfaces. Both the Maxwellian and primary electrons undergo inelastic collisions with neutrals, resulting in the production of Xe ions and excited Xe neutrals and ions. It is, however, assumed that energy loss associated with the production of multiply charged Xe (XeIII, XeIV) and excitation of multiply charged Xe is negligible. This assumption is also valid as the threshold energy for electron impact XeII and XeIII production is 35 V and 70 V respectively<sup>7</sup>. In the model, ionization or excitation of XeI may only result from primary or secondary electron inelastic collisions with a neutral Xe. It is assumed that electron-ion ionization/excitation is negligible due to the low number of ions relative to neutrals in the discharge chamber. It is also assumed that the plasma is quasi-neutral, namely the ion density is equal to the total electron density and the total electron density is the sum of the maxwellian and primary electrons.

$$n_{tot} = n_i \quad (2)$$

$$n_{tot} = n_M + n_P \quad (3)$$

The final two assumptions are that ions are cold relative to electrons, with a temperature of 0.05eV, and that volume averaged double ion production in the discharge plasma is negligible<sup>8</sup>, and as such is ignored in the calculations. The latter assumption is marginal, at high propellant utilization efficiencies where the discharge voltage may increase, but elimination from the analytical model was made to allow for explicit determination of all parameters. As ion engines are typically operated at 90% propellant utilization efficiency, where the primary electron energy is well below the threshold voltage for double ionization, this assumption is valid<sup>7</sup>. Although there are no measurements of ion temperature in the NSTAR thruster, ions are assumed to be born with the gas temperature during ionization. The gas temperature is essentially the wall temperature, 300°C, therefore an ion temperature of 0.05 eV is reasonable<sup>8</sup>.

### B. Plasma Confinement

Before the analytical model was developed, the theory for electron and ion confinement in the discharge plasma was formulated. A primary motivation for this research was the lack of such a theory applicable to ion thruster design and operation. In the 1970's and 1980's however, there was an extensive amount of basic plasma physics research in magnetic confinement for high power fusion containment. As such, this area was revisited for application to the low temperature and density plasma regime of an ion thruster.

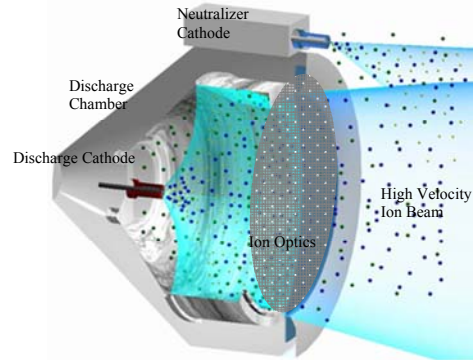


Figure 1. Ion thruster functional diagram.

### 1. Electron Confinement

In an electron bombardment ion engine, electrons are confined in a ring cusp magnetic field geometry. The magnetic field lines which originate and terminate at the cusps confine both the primary and Maxwellian electron populations. Electrons spiral around and along the field lines according to their Larmor radius until they eventually find and are lost to the magnetic cusp. Primary electrons are assumed to be mono-energetic with an energy that greatly exceeds the plasma electron temperature, allowing them to interact with the magnetic field in a single-particle manner. By definition they aren't part of the Coulomb-collision-produced Maxwellian distribution of the plasma electrons, and the plasma electrons and ions are assumed to not significantly affect their motion. As such the primary electrons are treated as a group of independent particles constrained to the field lines lost at a different rate than that of the Maxwellian electron population.

In a multi-pole cusp confinement engine, primary electrons are lost to the magnetic cusps in an area equal to twice the Larmor radius times the cusp length<sup>10</sup>. The magnetic cusp length is equal to the total circumference of all the magnet ring cusps inside the ion thruster.

$$A_p = 2R_L L_{cusp} \quad (4)$$

The total time the primary electrons spend in the discharge chamber is therefore a function of the volume of the containment device, the velocity of the electron, and the confinement area.

$$t_p = \frac{V}{A_p v_p} \quad (5)$$

The total distance traveled by a primary electron is thus equal to the product of the confinement time and electron velocity.

$$L_{confine} = v_p t_p \quad (6)$$

$$L_{confine} = v_p t_p = \frac{VeB}{2m_e v_p L_{cusp}} \quad (7)$$

Due to the presence of the neutral population, there is a probability of collision with a neutral, the mechanism by which ions are formed in the discharge chamber. Therefore, the probability that a primary electron is lost to the cusps is a function of the energy dependent total inelastic collision cross section, neutral density, as well as the electron confinement due to the ring cusp magnetic field. The probability that a primary electron is lost to the magnetic cusp may be computed from a differential equation approach. To determine the probability of electron loss as a function of time, a differential equation can be written to represent a differential diffusion of electrons in an increment of time, dt. Such an incremental diffusion is proportional to the inelastic collision frequency.

$$\partial J_{P,LOST} = J_{P,LOST} v_{inelastic} \partial t \quad (8)$$

Integrating Eq. (8) leads to the following expression for the primary electron current lost to the anode.

$$J_{P,LOST} = J_{po} e^{-v t} = J_D e^{-v_{inelastic} t} \quad (9)$$

The inelastic collision frequency is defined as follows.

$$v_{inelastic} = n_o \sigma_{inelastic} v_{prime} \quad (10)$$

Therefore, Eq. (9) may be rewritten as follows.

$$J_{P,LOST} = J_D e^{-n_o \sigma_o v_{prime} t} \quad (11)$$

An additional substitution can be made, recognizing that the product of  $v_{prime} t$  is simply the electron confinement length developed in Eq. (7). Therefore, Eq. (11) may be rewritten as follows.

$$J_{P,LOST} = J_D e^{-n_o \sigma_o L_{confine}} \quad (12)$$

The probability of primary electron loss is written as follows.

$$\text{Pr ob}_{P,LOSS} = \frac{J_{P,LOST}}{J_D} = e^{-n_o \sigma_o L_{confine}} \quad (13)$$

Eq. (13) indicates an exponential decrease with increasing neutral density, cross section, and confinement length. It is desired to minimize the loss of primary electrons to the anode as such losses reduce electrical efficiency. If a primary electron is lost prior to having an inelastic collision, the energy expended in creating the primary is lost. For a given engine operating point, the neutral density and cross section are fixed values. Therefore, to improve electrical efficiency the total confinement length must be increased. Equation (13) indicates that for NSTAR conditions and geometry, a cusp field strength of 2000 G is sufficient to ensure 99% of all primary electrons undergo an inelastic collision and only 1% are lost to the cusps. Such field strength is within the capability of commercially available permanent magnets.

The secondary or the Maxwellian electrons are confined according to the hybrid radius<sup>11</sup>. The hybrid radius is the square root of the product of the ion and Maxwellian electron Larmor radius.

$$R_{L,Hybrid} = \sqrt{R_{L,ion} R_{L,elec}} \quad (14)$$

The magnetic cusp loss area for primary electrons is equivalent to twice the hybrid diameter times the total cusp length<sup>10</sup>.

$$A_{e,therm} = 4R_{L,Hybrid}L_{cusp} \quad (15)$$

Unlike primary electrons, due to their significantly lower energy (velocity) as a result of energy exchange with ions during inelastic collisions, the plasma electron population motion is affected by the ion population and hence gyrates at the hybrid larmor radius. At the large hybrid radius described above, cross-field radial diffusion across field lines can occur for the secondary electron population if the magnetic field is not sufficiently strong.

Magnetic mirroring was also investigated to see if electron primary loss was reduced by mirroring. A magnetic mirror is based upon the invariance of the magnetic moment of a particle and conservation of kinetic energy. The supposed mirror for a particle would be defined by the saddle point magnetic field between cusps, and the stronger magnetic field at the cusps. Particles traveling on field lines between those areas could then conceivably be mirrored back from the cusps (throat). Conservation of the magnetic moment and energy requires that as particle moves from an area of weak magnetic field to stronger magnetic field, its perpendicular velocity component must increase and parallel component decrease. Therefore, for mirroring to occur,  $v_{\perp}^2$  goes to zero at the throat, and the particle is reflected back towards the saddle point. Not all particles in a magnetic mirror, however, are confined. There is a region of velocity space called the loss cone, inside of which particles are lost the magnetic cusp<sup>9</sup>. For the ion thruster, the loss cone angle is on the order of 5 degrees which suggests that a large number of electrons should be magnetically mirrored from the cusp region. Therefore the primary electron confinement length calculated previously can be interpreted as the number of bounces it must make before being lost to a cusp.

## 2. Ion Confinement

Enhancing magnetic ion confinement is vital to minimizing overall discharge loss as reducing the number of ions lost to the walls reduces the discharge power requirements. Ions are charged particles, but due to their relatively large mass and large gyro radius relative to the discharge chamber dimensions, they are not magnetically constrained to the field lines. Although ions are lost to the magnetic cusps, ion diffusion to the anode wall is the primary mechanism for their loss. Diffusion in a plasma is driven primarily by particle density gradients. In the absence of a strong electric field, ions will tend to drift to low density regions in the plasma, eventually making their way to the anode where the plasma density is zero. Although there is an axial electric field, established by the difference between the plasma potential and cathode common potential of the screen grid, its magnitude is not sufficient to prevent the loss of ion current to anode walls in the nominal NSTAR thruster. The rate at which diffusion occurs depends on many factors, including the degree of ionization of the plasma, the presence and strength of a magnetic field and the mass and charge of the diffusing particle. Classical and neoclassical diffusion in a magnetic field are not relevant to the ion thruster discharge plasma, as those constructs assume only coulomb collisions, and have no functional dependence on neutral-charged particle momentum transfer collisions. Therefore, only relations for diffusion in partially ionized plasmas are relevant.

In the absence of a magnetic field, ions diffuse via random walk collisions with a step length equal to their mean free path and as a result of ambipolar electric fields brought about by localized density gradients in the Maxwellian electron population. In the presence of a magnetic field, however, ions diffusion is magnetically constrained as demonstrated by previous researchers<sup>10,11</sup>. The effect of the magnetic field must therefore manifest itself in the random walk diffusion process and/or in the ambipolar electric fields generated by the Maxwellian electron

population. The probability that an ion will have a collision prior to its recombination at the anode wall is virtually zero, suggesting that the cyclotron gyration of the ion does not reduce radial diffusion to the anode wall. Therefore magnetic confinement of ions must be due to the requirement of quasineutrality in the discharge plasma. As electrons are light, their motion is governed by electron cyclotron gyration about the field lines as they drift towards the magnetic cusps. As electrons leave an area, the deficit of negative charge will set up an electric field that will attract ions. Therefore, ions will follow electrons in their magnetically constrained motion in order to shield out electric potentials that would otherwise exist due to electron magnetic confinement. The ion and electron number density profiles presented in Ref. 5 support this physical explanation. In more simplistic terms, the fact that ions are electrostatically confined by the plasma electrons is simply the requirement that diffusion of the plasma must be ambipolar.

In order to develop an analytical formalism for the electrostatic confinement of ions by the secondary electrons, we can recognize that random walk diffusion does apply to the secondary electron population. As shown experimentally by Koch and Matthieussent, the plasma electrons, in the presence of ions and a magnetic field actually gyrate at the hybrid gyro-radius<sup>11</sup>.

$$R_{L,hybrid} = \sqrt{R_{L,ion} R_{L,max}} \quad (16)$$

As ions are confined to the electrons, it is intuitive to think of the motion as an ion-electron pair walking in the direction opposite the density gradient.

The random walk process may now be applied to the diffusion of the ion-electron pair whose motion is defined by the hybrid Larmor radius. Chen shows, due to the presence of a magnetic field, the fluid equation of motion can be used to solve for the perpendicular velocity component resulting in the mobility and diffusion coefficients shown in Eqs. (17) and (18)<sup>9</sup>.

$$D_{\perp} = \frac{kT}{mv\nu \left[ 1 + \left( \frac{\lambda_m}{R_L} \right)^2 \right]} \quad (17)$$

$$\mu_{\perp} = \frac{q}{mv\nu \left[ 1 + \left( \frac{\lambda_m}{R_{L,i}} \right)^2 \right]} \quad (18)$$

The perpendicular diffusion and mobility coefficients are reduced by the factor  $1 + \left( \frac{\lambda_m}{R_{L,i}} \right)^2$ , in the presence of a magnetic field as compared to magnetic field free diffusion<sup>9</sup>. Therefore, the diffusion and mobility coefficients are proportional to  $B^{-2}$  and may be rewritten as follows for  $R_L \gg \lambda_m$ , where  $\lambda_m$  is 2.48 m and  $R_L$  is a 1 to 7cm, depending on the closed contour strength for the NSTAR discharge plasma.

$$D_{\perp} \approx \frac{v^2}{\nu n \sigma \left( \frac{1}{n \sigma R_L} \right)^2} = R_L^2 \nu n \sigma = R_L^2 \nu = \frac{R_L^2}{\tau} \quad (19)$$

$$\mu_{\perp} \approx \frac{q}{\nu n \sigma \left( \frac{1}{n \sigma R_{L,i}} \right)^2} = \frac{q R_L^2 n \sigma}{\nu} = \frac{q R_L^2 \nu}{\nu^2} = \frac{q R_L^2}{\nu^2 \tau} \quad (20)$$

It is clear that mobility coefficient is orders of magnitude less than the diffusion coefficient, due to the presence of  $\nu^2$  in the denominator. It is also clear that increasing the magnetic field strength, will reduce both plasma electron and ion diffusion, by reducing the effective larmor radius. In terms of the random walk mechanism, the electron-ion motion now walks at a path length equal to the hybrid larmor radius. As the charge particle is confined to gyrate

about a field line  $N \sim \frac{\lambda_m}{R_L}$  times until it has a collision, the step length between collisions is the Larmor radius.

Depending on where in the discharge chamber the ion is, the value of the magnetic field, and thus the larmor radius differs. In order to calculate a 0D effect of magnetic ion confinement, a design parameter for the magnetic field must be chosen to calculate the probability that ions produced in the discharge chamber are lost to the walls by diffusion across magnetic field lines. The minimum closed magnetic contour is used to define the radius of gyration for the approach developed here. The software MAXWELL 2D by Ansoft<sup>®</sup> was used to model the magnetic field of the NSTAR thruster for both the nominal and modified magnetic field designs investigated.

Random walk electron-ion diffusion is governed by a step length between collisions that is the hybrid larmor radius not the elastic scattering mean free path<sup>9</sup>. The probability that an ion diffuses an incremental area,  $dA$ , in a collision time,  $\tau$ , can be represented by a differential equation.

$$\partial J_{i,LOSS} = \frac{J_{i,LOSS}}{D_{\perp}} \partial A \quad (21)$$

Integrating and manipulating Eq. (21) leads to the following equation for the ion current lost to the anode.

$$J_{i,LOSS} = J_{io} e^{-D_{\perp}\tau A} \quad (22)$$

Using Eq. (22) and substituting Eq. (19), the probability an ion diffuses an area  $A$  is as follows.

$$Prob_{loss} = \frac{J_{i,LOSS}}{J_{io}} = \exp\left[-\frac{A}{R_{L,Hybrid}^2}\right] \quad (23)$$

The area  $A$ , that the ion must diffuse to be lost, is not intuitive. However, if we think of diffusion as 1D process to the wall, in an incremental distance  $dx$ , we can rewrite Eq. (21) and redo the integration as follows.

$$Prob_{i,loss} = \frac{J_{i,LOSS}}{J_{io}} = \exp\left[-\frac{d_{anode}}{R_{L,Hybrid}}\right] \quad (24)$$

Equation (24) shows us that under the pretext of a 0D model, and in the limit of  $R_L \gg \lambda_m$ , linear ion diffusion and loss is purely a function of the effective (hybrid) larmor radius and the distance it must travel before it reaches the wall, assuming its motion is obeying that of the magnetically confined secondary electron population, due to electrostatic attraction. This was shown with experimental spatially resolve Langmuir probe measurements in Ref. 5.

It is also interesting to note that use of Eq. (24) results in diffusion with a  $\frac{1}{B}$  dependence, which has been shown empirically to be the case for diffusion in the presence of a magnetic field by other plasma physics researchers<sup>9</sup>.

### III. Analytical Model

#### A. Power Balance Approach

The model developed is based on a steady state electrical power and particle balance to the discharge plasma<sup>6</sup>. The input power to the discharge chamber is equivalent to the output power that leaves the chamber. The power into the chamber is derived from the primary electron input into the chamber, which is related to the discharge supply output less the power needed to operate the hollow cathode.

$$P_{in} = J_D (V_D - V_C) \quad (25)$$

Energy from the primary electrons is either lost due to recombination with the anode walls or it is transferred to the propellant by ionization and excitation. Following a collision, the remaining energy goes into the Maxwellian population.

$$P_{in} = P_{ion} + P_{excite} + P_{WALL} + P_{MAXWELLIAN} \quad (26)$$

Each one of these terms can be explicitly defined in terms of known quantities. The power expended in ionization and excitation is as follows.

$$P_{ion} = U_{ion} J_{ion} \quad (27)$$

$$P_{excite} = \sum U_j J_j \quad (28)$$

As various excitations can occur, a summation over all possible states is required. This is the most useful representation as the total excitation cross section data for XeI is readily available in the literature<sup>43</sup>. The power expended in primary electron loss to the wall is as follows.

$$P_{P,LOST} = J_{P,LOST} (V_D - V_C) \quad (29)$$

Substituting in Eq. (13) for primary electron utilization, we see that power loss due to primary electron loss has an exponential dependence on neutral density, the inelastic collision cross section, and the electron confinement length.

$$P_{P,LOST} = (V_D - V_C) J_D e^{-n_o \sigma_o L_{confine}} \quad (30)$$

The remaining power from the primary electrons that do have an inelastic collision is assumed to go into a secondary Maxwellian electron population.

$$P_{MAXWELLIAN} = \frac{3}{2} T_e J_M \quad (31)$$

The Maxwellian population of electrons has two sources, primary electrons that have undergone any inelastic collision, and electrons released in the ionization process. Therefore, the Maxwellian electron current may be written as follows.

$$J_M = J_{ion} + (J_D - J_{P,LOST}) = J_{ion} + J_D (1 - e^{-n_o \sigma_o L_{confine}}) \quad (32)$$

All equations must now be written in terms of known variables, namely the throttle point settings,  $V_D, J_B, m_m, \eta_u$ , and the dependent variable  $\varepsilon_b$ . Equations for excitation and ionization production rates can be written in terms of the percentages of the two electron populations relative to the total plasma density.

$$J_{ion} = n_o n_{tot} V e \left( \frac{n_m}{n_{tot}} \langle \sigma_{ion} v_m \rangle + \frac{n_p}{n_{tot}} \sigma_{ion} v_p \right) \quad (33)$$

$$J_j = n_o n_{tot} V e \left( \frac{n_m}{n_{tot}} \sum \langle \sigma_{excite} v_m \rangle + \frac{n_p}{n_{tot}} \sum \sigma_{excite} v_p \right) \quad (34)$$

As the plasma is assumed to be quasi-neutral the following is also true.

$$n_{tot} = n_i = n_p + n_m \quad (35)$$

$$\frac{n_m}{n_{tot}} = 1 - \frac{n_p}{n_{tot}} \quad (36)$$

To simplify the above equations further it is useful to introduce the dependent parameter,  $\varepsilon_b$ , the discharge loss.

$$\varepsilon_b = \frac{J_D V_D}{J_B} \quad (37)$$

The discharge loss represents the energy expended in the production of ions that contribute to beam current. Beam current is only a fraction of the total ion current that is actually produced. The total ion current,  $J_{ion}$  may leave the thruster as beam current, or may recombine on cathode potential surfaces, or recombine on anode potential surfaces. The ion current can therefore be written as follows.

$$J_{ion} = J_B + J_A + J_C = J_B + J_A + J_K + J_S \quad (38)$$

Ion current to cathode potential surfaces ( $J_C$ ) is the sum of current to the keeper ( $J_K$ ) and to the screen grid ( $J_S$ ). Ion current to the keeper is negligible, less than 1% of the total current, so it is ignored in this analysis. Ion current that passes through the optics assembly, as opposed to recombining on the screen grid, is a function of the grid transparency to ions. The transparency of the optics assembly to ions is a thruster design parameter, and may be taken as an input to the model. For the NSTAR grids, the value is approximately 0.8 as calculated by CEX2D code<sup>12</sup> and as measured during the ELT<sup>3</sup>. The transparency to ions is defined as follows.

$$\phi_i = \frac{J_B}{J_B + J_s} \quad (39)$$

Therefore, the ion current may be written in terms of the anode and beam current only.

$$J_{ion} = \frac{J_B}{\phi_i} + J_A = \frac{J_B}{\phi_i \left( 1 - \frac{J_A}{J_{ion}} \right)} \quad (40)$$

As discussed in the previous section, the probability that an ion is lost to the anode is a function of the ion larmor radius. Therefore, substituting Eq. (24), the ion current can be written as follows.

$$J_{ion} = \frac{J_B}{\phi_i \left( 1 - e^{-\frac{d_{anode}}{R_{L,Hybrid}}} \right)} \quad (41)$$

In order to obtain an expression for the discharge loss, Eq. (26) may now be written in terms of  $\epsilon_B$  and the equations developed above.

$$\begin{aligned} \epsilon_B J_B - \frac{\epsilon_B J_B}{V_D} V_C = U_{ion} J_{ion} + \sum U_{excite} J_{excite} + \epsilon_B J_B e^{-n_o \sigma_o L_{confine}} - \frac{V_C}{V_D} \epsilon_B J_B e^{-n_o \sigma_o L_{confine}} \\ + \frac{3}{2} T_e J_{excite} + \frac{\epsilon_B J_B}{V_D} \left( 1 - e^{-n_o \sigma_o L_{confine}} \right) \frac{3}{2} T_e \end{aligned} \quad (42)$$

Dividing by  $J_{ion}$ , solving for  $\epsilon_B$ , and substituting in the formulations for  $J_{ion}$  and  $J_j$  leads to the following expression.

$$\epsilon_B = \frac{\frac{J_B}{\phi_i \left( 1 - e^{-n_o \sigma_o L_{confine}} \right)}}{J_B} \left[ \frac{\frac{3}{2} T_e + U_{ion} + \sum U_{excite} \left( \frac{n_m}{n_{tot}} \sum \langle \sigma_{excite} v_m \rangle + \frac{n_p}{n_{tot}} \sum \sigma_{excite} v_p \right)}{\left( \frac{n_m}{n_{tot}} \sum \langle \sigma_{ion} v_m \rangle + \frac{n_p}{n_{tot}} \sum \sigma_{ion} v_p \right)} \right] \left( 1 - e^{-n_o \sigma_o L_{confine}} \right) \left( 1 - \frac{V_C + \frac{3}{2} T_e}{V_D} \right) \quad (43)$$

Equation (43) is the expression for the discharge loss in terms of  $n_o$ ,  $T_e$ ,  $J_A$ ,  $v_p$ ,  $n_m/n_{tot}$ , and  $L_{confine}$ . The confinement length and anode current have been previously defined. The remaining variable will be solved for in the following subsection allowing an explicit expression for the discharge loss for any given ring cusp thruster design and operating conditions. Comparison of this 0D model to experimental testing data is discussed in section IV.

## B. Plasma Parameters

The primary electron velocity determination is straightforward.

$$v_p = \sqrt{\frac{2e(V_D - V_C)}{m_e}} \quad (44)$$

The neutral density may also be written in terms of known parameters, derived from neutral particle flux in free molecular flow.

$$Flux = \frac{n_o}{4} \sqrt{\frac{8kT_o}{\pi m_{Xe}}} \dots \left[ \frac{particles}{Area - time} \right] \quad (45)$$

Relating this to total Xe mass flow rate through the grids and propellant utilization is also straightforward as described in Ref. 6.

$$\dot{m} = \frac{m_{Xe}}{e} J_B + Flux * A_g \phi_g = \frac{m_{Xe} J_B}{e} + \frac{n_o}{4} \sqrt{\frac{2kT_o}{m_{Xe}}} A_g \phi_g = \frac{m_{Xe} J_B}{e \eta_u} \quad (46)$$

Solving for  $n_o$  yields Eq. (47).

$$n_o = \frac{4J_B}{eA_g \phi_g \sqrt{\frac{2kT_o}{m_{Xe}}}} \frac{(1 - \eta_u)}{\eta_u} \quad (47)$$

The primary to total electron density ratio may also be solved in terms of the known parameters. From quasineutrality, we know the ion current density is equivalent to the total electron density. From Ref. 13 we have the following expression for the beam current.

$$J_B = 0.6n_i e A_g \phi_i \sqrt{\frac{kT_e}{m_{Xe}}} \quad (48)$$

Taking Eq. (33), substituting in Eq. (48), and recognizing that  $n_i = n_{tot}$ , yields the following expression.

$$\frac{0.6eA_g \sqrt{\frac{kT_e}{m_{Xe}}}}{\left(1 - \frac{J_A}{J_{ION}}\right)} = n_o V e \left[ 1 - \frac{n_p}{n_{tot}} \right] \langle \sigma_{ion} v_m \rangle + \frac{n_p}{n_{tot}} \sigma_{ion} v_p \quad (49)$$

Solving for  $\frac{n_p}{n_{tot}}$  and substituting  $\frac{J_A}{J_{ION}}$  from Eq. (41) and for  $n_o$  from Eq. (48) leads to the following.

$$\frac{n_p}{n_{tot}} = \frac{\left[ \frac{0.6eA_g^2 \phi_g k \sqrt{T_e T_o}}{2J_B (1 - \left(\frac{1 - \eta_u}{\eta_u}\right) m_{Xe} V)} - \langle \sigma_{ion} v_m \rangle \right]}{\left( \sigma_{ion} v_p - \langle \sigma_{ion} v_m \rangle \right)} \quad (50)$$

The Maxwellian to total density ratio and the primary to Maxwellian density ratio is easily computed Eq. (50) and (36).

An expression for Te is not as straightforward as the previous terms. Instead a derivation of the Maxwellian averaged ionization reaction rate is obtained. Equation (33) may be rewritten by solving for  $\langle \sigma_{ion} v_m \rangle$ , dividing by  $n_m$ , and substituting in Eq. (41).

$$\langle \sigma_{ion} v_m \rangle = \frac{n_p}{n_m} \left( \frac{J_B}{\phi_i \left( 1 - e^{-\frac{d_{anode}}{R_{L,Hybrid}}} \right)} - \sigma_+ v_p \right) \quad (51)$$

In order to determine  $T_e$ , Eq. (51) is solved for  $\langle \sigma_{ion} v_m \rangle$  and set equal to Eq. (55). Using a polynomial curve fit for  $\langle \sigma_{ion} v_m \rangle$ , in terms of  $T_e$ , a Newtonian solver can be used to explicitly determine the value of  $T_e$  for a given thruster geometry, operating point ( $V_d, J_B, \eta_u$ ), and magnetic field design. The prediction of  $T_e$ , as a function of the minimum closed magnetic contour is discussed in section IV. The prediction of  $T_e$  as a function of  $\eta_u$ , for specific magnetic field designs is also discussed in section IV. The functional dependence is clear, as the magnetic field is increased, ion loss reduces and the bulk plasma electron temperature is reduced. For a given magnetic field design, as the propellant utilization is improved,  $T_e$  increases. With an explicit determination of  $T_e$ , all remaining parameters may be calculated, including plasma density ratios and discharge loss.

## IV. Comparison of Theory with Experiment

### A. Experimental Measurements Summary

Bulk performance and plasma parameter measurements for four separate NSTAR thruster magnetic field designs were obtained. Details on the engine modifications and test setup can be found in Ref. 5. For each case, the laboratory model NSTAR engine, named the NKO1 thruster, was physically modified by the addition/replacement of permanent magnets. The goal of the magnetic studies was to determine the dependence of plasma confinement and plasma uniformity on the strength and shape of the imposed ring-cusp magnetic field. The four cases investigated served to parametrically determine the individual effects of adding an additional magnetic cusp, increasing the magnitude of the minimum closed magnetic contour line, and varying the magnetic field geometry with respect to the anode wall; all design parameters captured in the 0D model.

CASE	NUMBER OF RINGS	CLOSED CONTOUR (G)
V1 (baseline)	3	20
V2	4	30
V3	4	50
V4	3	50

**Table 1. Summary of NSTAR engine tests<sup>5</sup>.**

Table 1 is a summary of the cases investigated. The nominal case, V1, is the 3-ring cusp engine configuration that was used for the DS1 mission and extended life test<sup>3</sup>. Cases V2 and V3 are 4-ring cusp versions of the NSTAR thruster. In case V2, a magnet ring was added to the center of the conical section of the discharge chamber. This design closed the 30G contour, a 10 G improvement over V1. The primary purpose of this configuration was to measure the effect that adding another cusp and pushing the minimum closed contour closer to the anode wall had on plasma uniformity. Case V3, in addition to having a conical segment magnet ring and a new cathode ring, also strengthened the middle ring cusp magnetic field by adding a ring of magnets directly over the existing middle ring. The resultant magnetic field closed the 50G contour. Case V3 was used to determine the effect of increasing the closed contour value, but trading it with a smaller magnetic field free region than V2. Case V4 is a 3-ring cusp NSTAR engine, but with a strengthened middle magnet ring (as in V3), allowing closure of the 50G magnetic contour line. V4 was used to separate the effects of physically adding an additional cusp from increasing the magnetic contour closure and increasing the field free volume. All configurations were modified to have alternating polarity cusps. For each of these cases, a 2D map of the magnetic field and magnetic contours was computed with the software MAXWELL 2D. The individual cusp magnetic field strength's was also measured with a Gauss meter. Measurements were taken for the TH15 operating point for each configuration. Discharge loss curves were generated for TH15 operation, to allow comparison of the actual performance to the predicted performance of the analytical model for all cases in investigated. This data set is used to determine the validity of the ion and electron confinement theory developed in section II.

## B. Model Results

DISCHARGE PARAMETER	V1	V3	V4
$T_e$ (eV)	5	5	5
$n_p/n_m$	0.09	0.09	0.09
$T_i$ (eV)	0.05	0.05	0.05
$J_B$ (A)	1.76	1.76	1.76
$V_D$ (V)	25.6	25.5	25.1
$V_C$ (V)	8	8	8
$L_e$ (m)	17.2	12.8	21.1
$f_A$	0.43	0.18	0.26
$B_{\text{contour,closed}}$	20	50	50
$d_{\text{Anode}}$ (cm)	2.3	1.9	1.5

**Table 2. 0D Model input parameters.**

The 0D analytical model discussed in section III was used to predict the performance of cases V1 and V3, and V4. Discharge loss versus mass utilization curves were obtained experimentally and compared to the model predictions for cases V1, V3, and V4. Case V2 was not modeled as the experimental discharge loss data collected was not taken at a constant discharge voltage and cannot be directly compared to the model. The input parameters for each case are shown in Table 2. The primary electron confinement length was computed from Eq. (11) for each configuration, based on the measured/predicted cusp strength magnetic field and the dimensions of each magnet ring. The ion loss fraction was calculated from Eq. (41), based on the Maxwell 2D simulations of the closed contour line to anode wall minimum gap and the hybrid larmor radius. The electron temperature and primary electron fraction were assumed to be 5eV and 9% respectively. Although an equation was developed to calculate the volume averaged electron temperature, it is not used in this model as much of the ionization occurs in the cathode plume, where an average value of 5eV was measured for all cases<sup>5</sup>. The primary-electron-to-total-density ratio of 9% is computed from Eq. (52), based on an electron temperature of 5 eV. An ion temperature of 0.05 eV is used to calculate the ion velocity and larmor radius. As discussed previously the ions are assumed to be lost to thruster surfaces (recombination) or are extracted as beam ions from the thruster and are assumed to not gain energy as they flow collisionlessly towards the grids or anode.

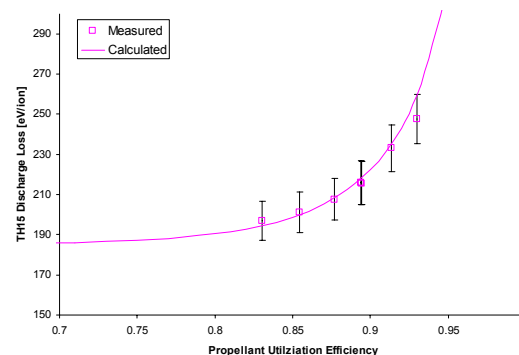


**Figure 2. Comparison of measured to predicted discharge loss at TH15 for the nominal configuration.**

A comparison of the predicted and measured discharge loss at TH15 is shown in figures 2 to 4 for cases V1, V3, and V4, respectively. All three predictions compare well to tests data over the propellant utilization range investigated. Figure 2 is a comparison of the predicted discharge loss curves. The nominal case and case V4 differed by a translation in the Y axis, but little change in the shape of the curve. Case V3 and V1 differed in both shape and magnitude. The translation in Y is related to the ion loss which is independent of propellant utilization or neutral density, as the secondary electron diffusion is dependant on the hybrid larmor radius only. The change in shape of the curve from V1 to V3 is due to the exponential dependence of primary electron confinement, on the magnetic field and neutral density (propellant utilization). This suggests that case V4 had similar primary electron confinement to case V1, and improved ion confinement. Case V3 had reduced primary electron confinement, but improved ion confinement, as compared to case V1. It is important to point out that the model was run assuming a fixed beam current (1.76A) and discharge voltage (see Table 2). Therefore, changes in discharge loss were due to changes in discharge current only. It is fair to say that the model adequately predicts the discharge loss over the measured propellant utilization range for all cases tested, suggesting the energy loss formulation used in the 0D model is fundamentally accurate.

There are four mechanisms for energy loss in the model.

1. Primary electron Utilization
2. Ion Loss to the Anode
3. Plasma Electron Loss to Anode
4. Hollow Cathode Operation

The primary electron utilization was determined from the electron containment length which is a function of the total cusp length and cusp magnetic field strength. Figure 6 is a plot of primary electron utilization factor (percent of primary electrons that have an inelastic collision before being lost to the anode) versus electron confinement length. The benefit of increasing confinement length begins to level off at about 14m, due to the exponential dependence of primary electron inelastic collision frequency. The experimental cases are also included on the graph for reference. Case V4 had the most efficient use of primary electrons, due to the strengthened middle magnet ring, and no net increase in cusp length versus the nominal case. At a propellant utilization efficiency of 90%, 95%

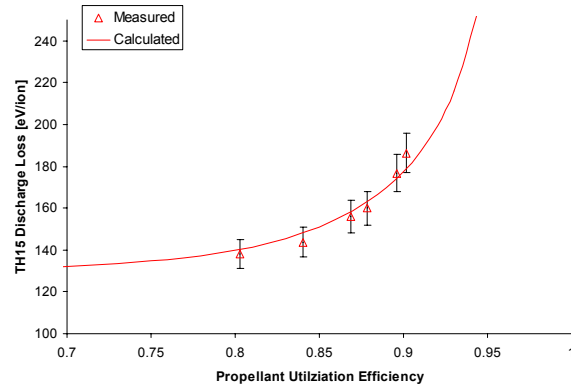


**Figure 3. Comparison of measured to predicted discharge loss at TH15 for case V3.**

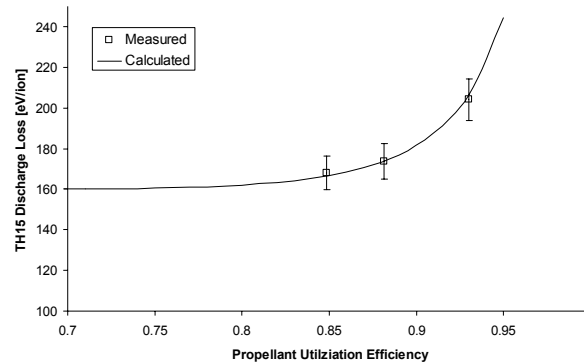


**Figure 4. Comparison of measured to predicted discharge loss at TH15 for case V4.**

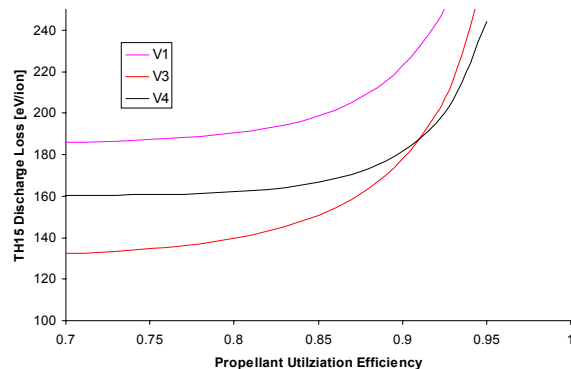


**Figure 5. Comparison of predicted discharge loss at TH15 for all cases.**

of primary electrons underwent an inelastic collision for V4. Case V3 had the least efficient use of primary electrons, due to the addition of the conical cusp (increase in the total cusp length), and the use of a stainless steel shim on the front magnet ring that reduced the cusp strength on the front ring from 1100 to 800G, in an attempt to increase the field free volume in the vicinity of the grids. In case V3, only 85% of primary electrons underwent an elastic collision, with 15% lost to the magnetic cusps. For the nominal case, with a primary electron containment length closer to that of case V4, 92% of primary electrons underwent an inelastic collision according to the model, at 90% propellant utilization. It is clear that the addition of magnet rings must be traded with the loss of primary electrons to the cusps. This issue could be mitigated by strengthening all the cusps to 2000 G, however, that must be traded with maintaining a relatively field free volume in the discharge chamber.

In spite of the reduced primary electron confinement of case V3, the total discharge loss was 20% less than the nominal case, and equal to case V4. This is because the ion loss to the anode was lowest for case V3. Only 18% of the total ion production in the discharge chamber was lost to the anode, as compared to 43% for the nominal case, and 26% for case V4. The ion loss factor,  $f_A$ , is both a function of the magnetic contour strength (the hybrid gyro radius) as well as the distance of the contour from the anode. Given the exponential dependence of ion loss fraction on this product, both decreasing the hybrid gyro radius and/or distance from the anode wall will improve ion confinement. There is a tradeoff in that increasing the distance from the anode wall will reduce ion loss, but it will also reduce the magnetically field free volume reducing plasma uniformity. Similarly, if the strength of the magnets is increased, the higher Gauss contour lines will push further into the chamber, having a similar effect. Figure 7 is a plot of the ion loss fraction as a function the closed magnetic contour value at 1, 2, and 3 cm spacing from the anode wall. The closer the closed contour line is to the anode wall, the more dramatic effect increasing its value has on ion confinement. This was demonstrated by cases V3 and V4, which closed the 50G contour line. In case V3, the contour was located 1.9 cm from the anode wall as opposed to 1.5 cm for case V4. This resulted in the improved ion confinement for V3 versus V4.

Energy used to operate the hollow cathode is also a major loss mechanism for the NSTAR thruster. Eight volts was used to represent the plasma potential from which the electrons were supplied for all cases investigated<sup>14</sup>. This potential was also assumed to be constant over the investigated propellant utilization range of 95 to 80%. The limit to this assumption is that the hollow cathode will begin to operate less efficiently and eventually go unstable as the cathode flow rate is reduced. As the 0D model does not take hollow cathode efficiency as a function of propellant utilization into account; it is only valid over a range where the cathode operation is stable. However, as ion engines are typically only operated in the vicinity of 90% propellant utilization, far from the regime where the hollow cathode goes unstable, this effect does not need to be captured for a performance model to be representative.

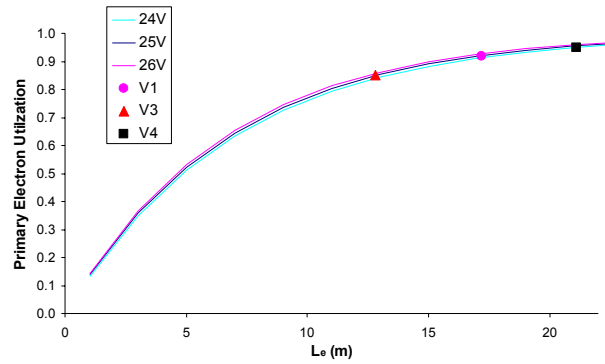


**Figure 6. Primary electron utilization as a function of the magnetic confinement length for different discharge voltages.**

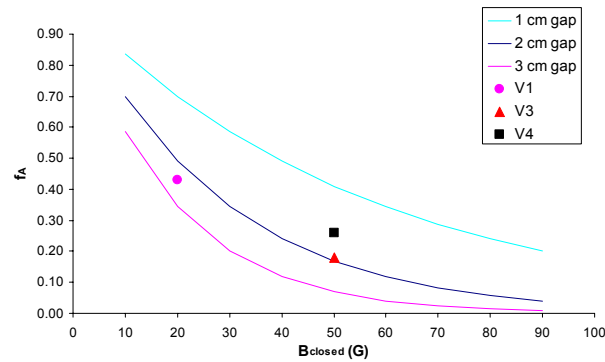


**Figure 7. Ion loss fraction as a function of the closed magnetic contour strength for different anode to contour spacing.**

### C. Plasma Parameters

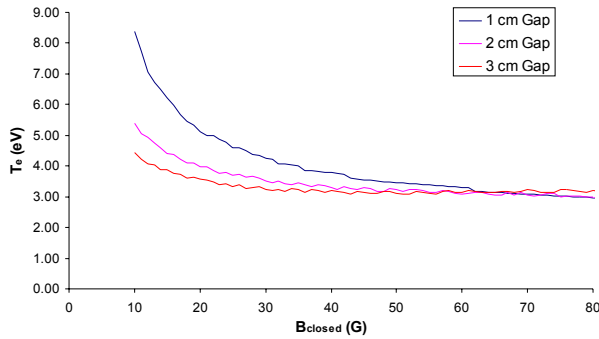


**Figure 8.** Volume averaged electron temperature at TH15 as a function of the closed contour strength and anode gap.

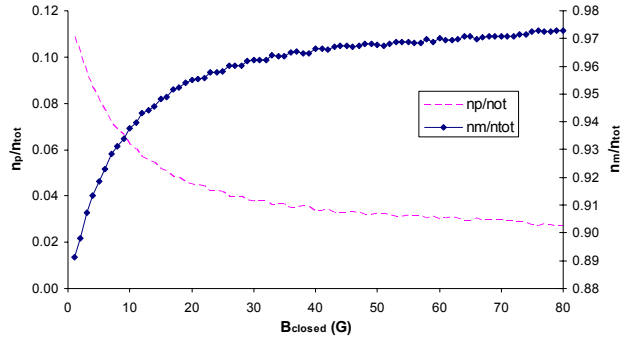


**Figure 9.** Volume averaged  $n_p/n_{tot}$  and  $n_m/n_{tot}$  at TH15 as a function of closed contour strength for a 2 cm gap.

Although the plasma parameter equations of section III were not used in the calculation of ionization rate, due to the non-uniform or peaked nature of the plasma, it is still interesting to see how the model predictions of volume averaged plasma parameters change as a function of propellant utilization and magnetic field. Figure 8 is a plot of TH15 electron temperature versus closed contour magnetic field strength, for 1, 2, and 3cm distance from the anode at 90% propellant utilization. As the magnetic field strength and therefore ion confinement is increased, the discharge loss decreases, and the discharge current is reduced for a fixed beam current. As a result, the energy of the primary electrons decreases and the Maxwellian electron temperature decreases, logarithmically, and levels off at about 3eV. Figure 9 is a plot of primary-to-total and Maxwellian-to-total density ratio as a function of magnetic field strength, assuming a fixed distance from the anode (2cm). As the magnetic field strength is increased, the fraction of primary electrons in the total electron population decreases, therefore the plasma becomes more Maxwellian.

Figure 10 is a plot of electron temperature as a function of propellant utilization, for fixed magnetic contour line closure values. For high utilization or low neutral number density, the temperature of the Maxwellian population increases to provide the required level of ionization. The sensitivity of electron temperature to changes in neutral density is higher for low field strength or poor ion confinement. Figure 11 is a plot of primary to total electron density as a function of propellant utilization, for fixed magnetic contour line closure values. For high utilization, or low neutral density, the primary electron fraction increases, largely due to the increase in discharge current, to

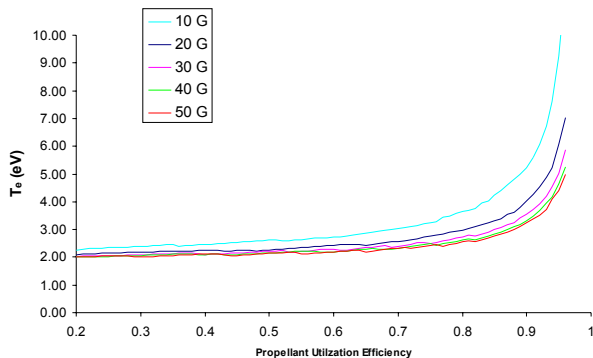


**Figure 10.** Volume averaged electron temperature at TH15 as a function of propellant utilization for various closed contour strengths.

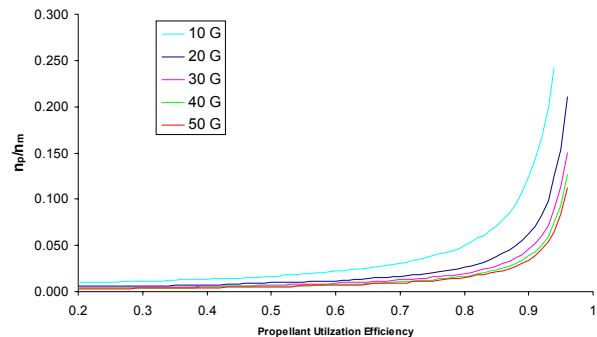


**Figure 11.** Volume averaged  $n_p/n_{tot}$  at TH15 as a function of propellant utilization for various closed contour strengths.

provide the required level of ionization.

In summary, the model indicates that plasma parameters are highly dependent on the magnetic field configuration, and that their sensitivity to changes in neutral density is reduced with increasing magnetic strength

## V. Discussion of Plasma Uniformity

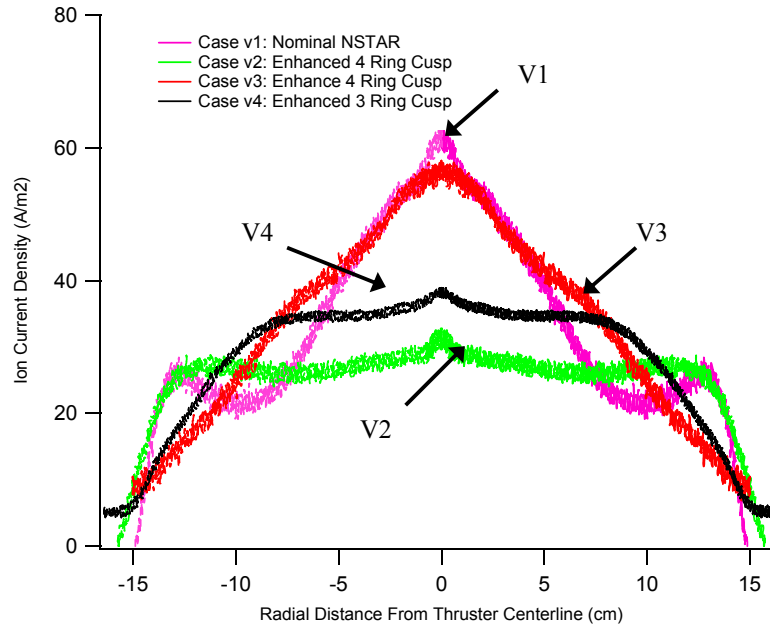


**Figure 13. Ion current density comparison for all cases investigated for 14cm downstream of cathode (near grid region) showing mirror image of the Langmuir probe data from 0 to -15cm<sup>5</sup>.**

Although the 0D model cannot predict the plasma uniformity, as that requires a 2D treatment<sup>12</sup>, the theory developed can be applied qualitatively to the ion saturation profiles from Ref. 5. Figure 13 is a plot of the near grid region ion saturation profiles for all four cases investigated. Cases V2 and V4 had the most uniform plasma while cases V1 and V4 were highly peaked on axis. Inspection of the magnetic fields of each case indicates that plasma uniformity in the near grid region is primarily a function of the magnetic field structure in this region. Increasing the field free volume in the cylindrical region is critical for producing a flat beam profile. Conversely, reducing the field free volume in this region resulted in a peaked beam profile (V1 and V3).

The fractional ion loss to the anode is a function of the magnetic contour value and the location of that contour with respect to the anode. The 0D model only uses the minimum distance, as it is assumed that most ions flow to this region, essentially a field free anti-cusp region that attracts both secondary electrons and ions. The Maxwell 2D plots indicate that the conical region of the plasma actually closes the 60G contour line, with up to a 5cm gap between that contour and the anode wall, as opposed to the cylindrical region, where the contour line is as close as 1 cm from the anode. This suggests that ion loss in the discharge chamber may be concentrated in the cylindrical segment. Inspection of ion saturation profiles in both the conical and cylindrical segments does seem to support this theory. The experimental data does indicate that ion loss occurs primarily in the cylindrical region, and it is this loss that contributes to the peaked nature of the beam profile, in cases V1 and V3.

## VI. Conclusion

The objective of this research was to quantitatively understand and improve upon the confinement and production of the ion thruster discharge plasma by theoretical development of discharge plasma confinement theory validated by experimental measurements inside of an operating ion thruster. The results have shown that the primary electrical inefficiency in the nominal NSTAR thruster is insufficient containment and the loss of ions and plasma

electrons to the anode. The results have also demonstrated that ion confinement is dependent on the magnetic confinement of the Maxwellian electron population. As diffusion in the discharge plasma is ambipolar, ions are electrostatically confined to the electrons. Increasing the magnetic strength of the chamber's maximum closed contour line reduced the Larmor radius of the Maxwellian electrons and reduced cross field diffusion to the anode. As the fraction of ions that were lost to the anode was reduced, the discharge current to produce the same beam current was reduced for the enhanced NSTAR cases, increasing cathode life and reducing discharge loss.

The primary requirements for the magnetic design of any ion engine must be to minimize discharge loss and maximize the field free volume of the plasma, resulting in a flat beam profile. This is accomplished by the determination of the optimum number, strength, and location of magnetic cusps. Unfortunately, the state-of-the art engine was designed to minimize unit mass, and as a result the mass savings achieved by minimizing magnet weight resulted in a magnetic field that does not adequately confine or distribute the plasma, resulting in substantial performance and lifetime limitations. The improvements demonstrated above were accomplished via straightforward changes in the magnetic field, and should be made to ensure future and continued use of ion thrusters on NASA science missions.

### Acknowledgments

The author would like to acknowledge Dr. Dan Goebel, Al Owens, and Dr. Dennis Fitzgerald of the Jet Propulsion Laboratory, for assisting in the preparation and implementation of this research activity. The Jet Propulsion Laboratory, California Institute of Technology carried out the research described in this paper, under a contract with the National Aeronautics and Space Administration.

### References

- <sup>1</sup> J.R. Brophy, et al., "Ion Propulsion System (NSTAR) DS1 Technology Validation Report," JPL Publication 00-10, Oct. 2000.
- <sup>2</sup> J.R. Brophy, M. Marcucci, J. Gates, C. Garner, B. Nakazono, and G. Ganapathi, "Status of the Dawn Ion Propulsion System," AIAA-2004-3433, Jul. 2004.
- <sup>3</sup> A. Sengupta, et al., "The 30,000-Hour Extended-Life Test of the Deep Space 1 Flight Spare Ion Thruster, Final Report," NASA TP 2004-213391, Nov. 2004.
- <sup>4</sup> J.E. Polk, J.R. Anderson, J.R. Brophy, V.K. Rawlin, M.J. Patterson, and J.S. Sovey, "In Situ, Time-Resolved Accelerator Grid Erosion Measurements in the NSTAR 8000 Hour Ion Engine Wear Test," IEPC-97-047, presented at the 25th International Electric Propulsion Conference, Cleveland, OH, Aug. 1997.
- <sup>5</sup> A. Sengupta, "Experimental Investigation of Discharge Plasma Magnetic Confinement in an NSTAR Ion Thruster," AIAA-2005-4069, presented at the 41st Joint Propulsion Conference, Tucson, Arizona, July 2005.
- <sup>6</sup> J.R. Brophy, "Ion Thruster Performance Model", Ph.D. Dissertation, Colorado State University, 1984.
- <sup>7</sup> H. Tawara and T. Kato, "Total and Partial Ionization Cross Sections of Atoms and Ions by Electron Impact," Atomic Data and Nuclear Tables, Vol. 36, No. 2, March 1987.
- <sup>8</sup> A. Sengupta, et al., "The 30,000-Hour Extended-Life Test of the Deep Space 1 Flight Spare Ion Thruster, Final Report," NASA TP 2004-213391, Nov. 2004.
- <sup>9</sup> F.F. Chen, "Introduction to Plasma Physics and Controlled Fusion", Second Edition, Plenum Press, New York, 1984.
- <sup>10</sup> K.N. Leung, et.al, "Plasma confinement by localized cusps", Phys. Fluids 19 (7), p.1045 (1976).
- <sup>11</sup> C. Koch and G. Matthieussent, "Collisional Diffusion of a Plasma in a Multipolar and Picket Fence Devices," Phys. Fluids 26 (2) February 1983.
- <sup>12</sup> I. Katz, I.G. Mikellides, R. Wirz, J.R. Anderson, D.M. Goebel, "Ion Thruster Life Models," AIAA-2005-4256, 41st AIAA/ASME/SAE/ASEE Joint Propulsion Conference and Exhibit, Tucson, AZ, July 2005.
- <sup>13</sup> B. Chapman, Glow Discharge Processes, John Wiley & Sons, Inc., New York, 1980.
- <sup>14</sup> K. Jameson, D. Goebel, and R. Watkins, "Hollow Cathode and Keeper-Region Plasma Measurements", AIAA 2005-3667, presented at the 41st AIAA/ASME/SAE/ASEE Joint Propulsion Conference, Tucson, Arizona, 2005.